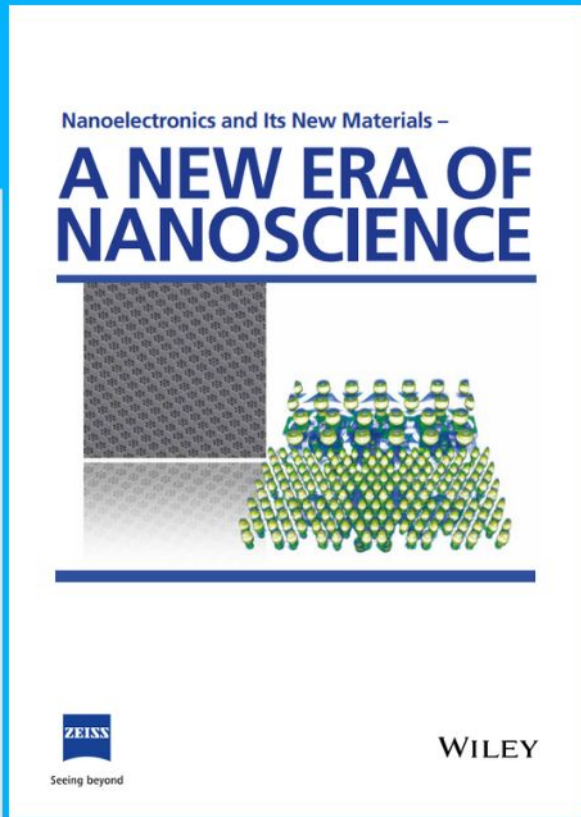




# Nanoelectronics and Its New Materials – A NEW ERA OF NANOSCIENCE



**Discover the recent advances in electronics research and fundamental nanoscience.**

Nanotechnology has become the driving force behind breakthroughs in engineering, materials science, physics, chemistry, and biological sciences. In this compendium, we delve into a wide range of novel applications that highlight recent advances in electronics research and fundamental nanoscience. From surface analysis and defect detection to tailored optical functionality and transparent nanowire electrodes, this eBook covers key topics that will revolutionize the future of electronics.

To get your hands on this valuable resource and unleash the power of nanotechnology, simply download the eBook now. Stay ahead of the curve and embrace the future of electronics with nanoscience as your guide.



Seeing beyond

**WILEY**

# High-Performance Pressure Sensors Based on Shaped Gel Droplet Arrays

Zhenwu Wang,\* Qianyu Cai, Lutong Lu, and Pavel A. Levkin\*

Polymer gel-based pressure sensors offer numerous advantages over traditional sensing technologies, including excellent conformability and integration into wearable devices. However, challenges persist in terms of their performance and manufacturing technology. In this study, a method for fabricating gel pressure sensors using a hydrophobic/hydrophilic patterned surface is introduced. By shaping and fine-tuning the droplets of the polymer gel prepolymerization solution on the patterned surface, remarkable sensitivity improvements compared to unshaped hydrogels have been achieved. This also showcased the potential for tailoring gel pressure sensors to different applications. By optimizing the configuration of the sensor array, an uneven conductive gel array is fabricated, which exhibited a high sensitivity of  $0.29 \text{ kPa}^{-1}$  in the pressure range of 0–30 kPa, while maintaining a sensitivity of  $0.13 \text{ kPa}^{-1}$  from 30 kPa up to 100 kPa. Furthermore, the feasibility of using these sensors for human motion monitoring is explored and a conductive gel array for 2D force detection is successfully developed. This efficient and scalable fabrication method holds promise for advancing pressure sensor technology and offers exciting prospects for various industries and research fields.

## 1. Introduction

Wearable electronics have experienced exponential growth in recent years, driven by the increasing demand for monitoring physiological data in healthcare.<sup>[1–4]</sup> Devices, such as pulse oximeters, heart rate monitors, and infrared thermometers, provide valuable insights into human health and well-being.<sup>[5]</sup> In addition to their sensing capabilities, wearable electronic devices must

also meet requirements for non-toxicity, biocompatibility, and comfort.<sup>[6–8]</sup> These demands have given rise to the development of lightweight and comfortable flexible electronics.<sup>[9–12]</sup> To meet these requirements, soft conductive materials, as the fundamental materials for flexible electronics, have garnered significant interest in the research community.<sup>[13,14]</sup> These soft conductive materials enable the conversion of deformation or force into electrical signals,<sup>[15,16]</sup> allowing for the detection of physiological signals like pulse, heart rate, and human movement.<sup>[17–19]</sup>

Conductive polymer gels, with tissue-like properties and customization capabilities for specific requirements, have found applications in various fields, including biomedical engineering,<sup>[20,21]</sup> soft robotics,<sup>[22,23]</sup> human-machine interface,<sup>[24,25]</sup> and wearable devices.<sup>[11,18,26]</sup> In wearable devices, conductive polymer gels usually serve as the active materials for pressure sensors, strain sensors as well as biosensors, which transfer external stimuli into electrical


signals.<sup>[27]</sup> Pressure sensors based on polymer gels offer several advantages over traditional sensing technologies. They possess conformability, allowing them to conform to irregular surfaces and adapt to different environments.<sup>[28,29]</sup> This unique characteristic enables their integration into wearable devices and the development of human-machine interfaces. Despite the progress made in the field, there are still significant challenges associated with the performance and manufacturing technology of polymer gel-based pressure sensors.<sup>[30,31]</sup> The performance of these sensors, in terms of sensitivity, response time, and stability, still needs improvement to meet the demands of various applications.

The microstructure design of active materials in pressure sensors has proven to be an efficient approach to enhance their performance.<sup>[32,33]</sup> Existing gel-based sensors are typically fabricated using molding or 3D-printing techniques, which face challenges in creating small or inverted structures.<sup>[34–36]</sup> A new and facile approach for universal polymer gel microengineering is thus important to uncover the full potential of polymer gels in wearable electronics and advance bioelectronic applications.

Here, we have developed a method for fabricating gel pressure sensors using a hydrophobic/hydrophilic patterned surface (Figure 1a). By leveraging the unique properties of this patterned surface, we can shape and fine-tune droplets of a polymer gel prepolymerization solution, followed by their polymerization. The

Z. Wang, Q. Cai, L. Lu, P. A. Levkin  
Institute of Biological and Chemical Systems-Functional Molecular Systems (IBCS-FMS), Karlsruhe Institute of Technology (KIT)  
Hermann-von-Helmholtz-Platz 1, 76344 Eggenstein-Leopoldshafen, Germany  
E-mail: wangzhenwuup@163.com; levkin@kit.edu

Z. Wang, Q. Cai, P. A. Levkin  
Institute of Organic Chemistry (IOC)  
Karlsruhe Institute of Technology (KIT)  
Fritz-Haber-Weg 6, 76131 Karlsruhe, Germany

 The ORCID identification number(s) for the author(s) of this article can be found under <https://doi.org/10.1002/smll.202305214>

© 2023 The Authors. Small published by Wiley-VCH GmbH. This is an open access article under the terms of the Creative Commons Attribution License, which permits use, distribution and reproduction in any medium, provided the original work is properly cited.

DOI: 10.1002/smll.202305214

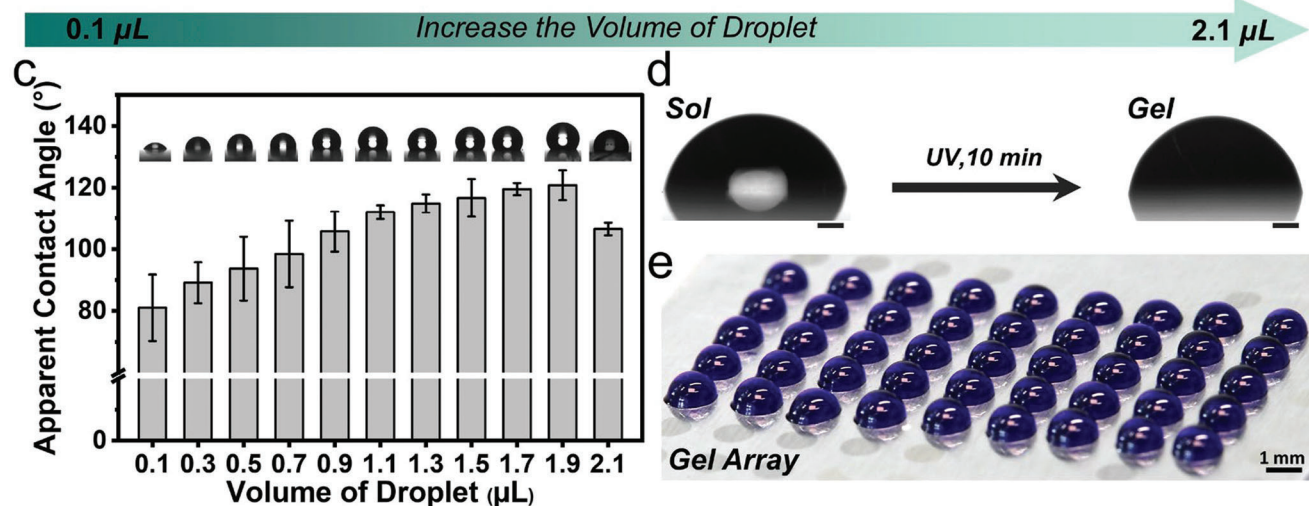
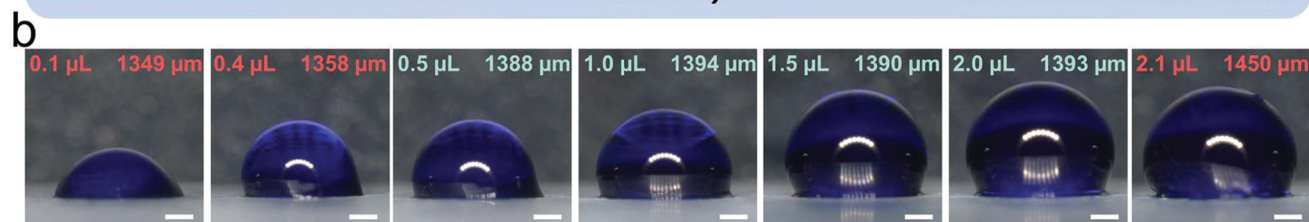
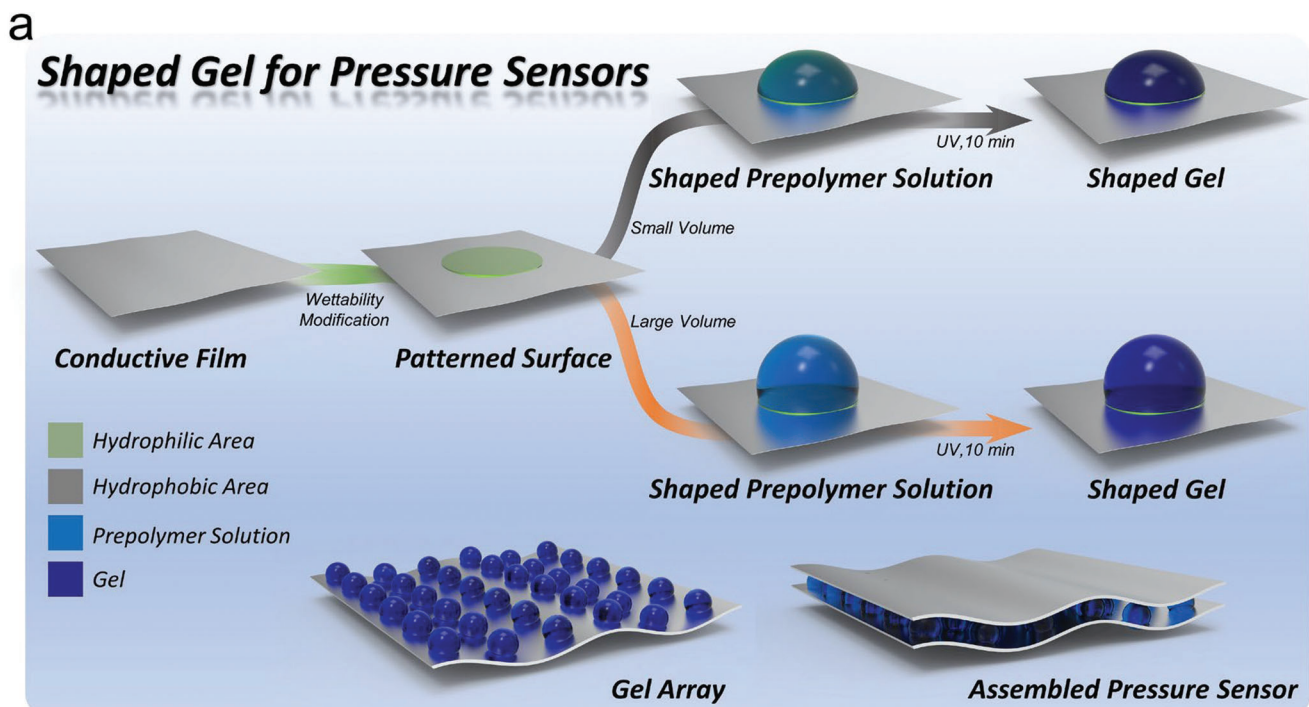


**Figure 1.** a) Schematic illustration of the workflow for fabricating pressure sensors using conductive gel droplets shaped by a hydrophobic/hydrophilic pattern on a conductive film. The shape of the prepolymer solution can be controlled by the hydrophobic/hydrophilic pattern and then transformed into a gel state to retain its shape. Precise control over the shape of the conductive gel can be achieved by adjusting the volume of the prepolymer solution. These shaped conductive gel droplets are subsequently assembled with another conductive film to create pressure sensors. In this configuration, the conductive gels act as soft active materials, converting applied pressure into changes in electrical signals through deformation. b) Photographs show gel droplets on a circular pattern with a diameter of 1400  $\mu\text{m}$ . The volume of the droplets varies from 0.1 to 2.1  $\mu\text{L}$ , and the corresponding droplet footprint diameter of the gel is indicated in the upper right corner of each image. c) The apparent contact angle of the shaped solution on the pattern with a diameter of 1400  $\mu\text{m}$  is measured as a function of volume. d) Photographs display the shaped prepolymer solution before and after UV polymerization. The shape of the solution is maintained upon polymerization, resulting in a gel structure. e) The photograph exhibits an array of conductive gels on an aluminum film with hydrophilic/hydrophobic patterns. Scale bars, unless otherwise noted, are 200  $\mu\text{m}$ .



resulting conductive gels exhibited remarkable improvements in sensitivity compared to unshaped hydrogels. Through comprehensive analysis of the pressure sensing performance, we conducted simultaneous measurements of applied pressure and electrical output signals. Notably, pressure sensors with a droplet volume of 1.5  $\mu\text{L}$  on a 1.4 mm pattern demonstrated significantly higher sensitivity ( $0.048 \text{ kPa}^{-1}$  for pressure up to 100 kPa), representing a five-fold enhancement compared to cylindrical sensor structures. Moreover, by optimizing the configuration of the sensor array, we achieved an uneven conductive gel array that exhibited a high sensitivity of  $0.29 \text{ kPa}^{-1}$  in the pressure range of 0–30 kPa, while maintaining a sensitivity of  $0.13 \text{ kPa}^{-1}$  within 30–100 kPa range. These findings demonstrate the potential of this approach in tailoring the sensitivity of gel pressure sensors for specific pressure ranges. Importantly, we explored the feasibility of applying these pressure sensors for human motion monitoring, highlighting their potential in the field of wearable electronics. Additionally, leveraging the scalability of our fabrication process, we successfully developed a conductive gel array for 2D force detection. This efficient and straightforward method opens up avenues for advancements in pressure sensors, presenting prospects for diverse industries and research fields.

## 2. Results and Discussion

### 2.1. Shaped Gels on the Patterned Surface

An aluminum tape was chosen as the model substrate for the droplet array due to its accessibility, flexibility, and high electrical conductivity. To modify the aluminum substrate, the surface was first treated with trichlorovinylsilane to functionalize it with vinyl groups. Then, the thiol-ene click reaction was performed using UV light and a quartz photomask to modify the surface with either 1*H*,1*H*,2*H*,2*H*-perfluorodecanethiol or 1-thioglycerol (Figure S1, Supporting Information). This method results in hydrophobic fluorinated areas with  $\theta_{\text{st}}$  of  $123^\circ$  surrounding the hydrophilic hydroxylated circular patterns with  $\theta_{\text{st}}$  less than  $6.9^\circ$ . The hydrophilic spots on the conductive surface were then filled with gel precursor solutions, whereby the combination of hydrophilic spot geometry and volume could define the shape of the droplets (Figure 1a). For the conductive gel model, we employed 2-hydroxyethyl methacrylate as the monomer for the polymer matrix and incorporated poly(ethylene glycol) diacrylate (PEGDA,  $M_n \approx 250 \text{ g}\cdot\text{mol}^{-1}$ ) as the chemical crosslinker to fabricate hydrogels through a one-step UV-induced radical polymerization (Experimental Section, Figure S2, Supporting Information). To emulate the electrical conduction of human tissues and avoid the rapid solvent evaporation, we chose a mixture (volume ratio = 1:1) of ethylene glycol and saline (0.9% w/v NaCl water solution) as solvent. Monitoring the weight loss of the conductive gels under ambient conditions for up to 72 h (Figure S3, Supporting Information) revealed that the inclusion of ethylene glycol effectively slowed down the evaporation process of the conductive gels. As the active soft material in pressure sensors, the stability of the conductive gels under ambient conditions for 72 h and its mechanically recoverable properties were also confirmed in Figure S4, Supporting Information.

Due to the repellency of the hydrophobic regions, the prepolymerization solution naturally remains confined within the hy-

drophilic circular pattern. As the volume of the liquid increases, the droplet shape on the hydrophilic pattern undergoes changes, characterized by an increase in the droplet footprint and apparent contact angle (Figure 1a). In Figure 1b, the prepolymerization solution of the conductive gels was placed on a hydrophilic pattern with a diameter of 1400  $\mu\text{m}$ , with variations in the volume of the solution. When the droplet volume is less than 0.4  $\mu\text{L}$ , the droplet footprint diameter is smaller than 1360  $\mu\text{m}$ , indicating that the liquid has not completely wetted the hydrophilic pattern. As the volume of the solution exceeds 0.5  $\mu\text{L}$ , the bottom diameter of the droplet increases up to 1388  $\mu\text{m}$  and maintains this diameter up to 2.0  $\mu\text{L}$  (1393  $\mu\text{m}$ ). With further increase in the solution volume, the liquid overflows from the hydrophilic area (at  $123^\circ$  of apparent contact angle), causing the droplet footprint diameter to reach 1450  $\mu\text{m}$ . The apparent contact angle of the droplet (Figure 1c) increases from  $80.9^\circ$  to  $120.8^\circ$ , upon droplet volume increase from 0.1 to 1.9  $\mu\text{L}$ . However, when the volume reaches 2.1  $\mu\text{L}$ , the apparent contact angle drops to  $106.5^\circ$ , indicating the movement of the contact line. Therefore, for the circular pattern with a diameter of 1400  $\mu\text{m}$ , the range of control for tuning the shape of the droplet spans from 0.5 to 2.0  $\mu\text{L}$ . Additionally, the ability of this method to retain the shape of a droplet during photoinitiated polymerization was demonstrated, as depicted in Figure 1d. The confined droplet exhibited minimal shape variation before and after 10 min of UV polymerization.

### 2.2. Sensing Property of Shaped Conductive Gels

The ionic conductivity and electrical stability of the conductive gels are demonstrated in Figure S5, Supporting Information, which serves as a validation for their electrical performance as soft active materials in pressure sensors. Specifically, the gels exhibit an ionic conductivity of  $0.018 \text{ S}\cdot\text{m}^{-1}$ , with a minimal change of less than 1% observed over a 24-h period in ambient conditions. Furthermore, in cyclic voltammetry measurements, the gels retain over 50% of their initial current density even after 10 000 cycles of scanning with 1 V. Based on the good electrical performance, the relation between shape and sensing property is revealed in Figure 2 and Figure S6, Supporting Information. According to the previous tuning range on the pattern with 1400  $\mu\text{m}$  diameter, 0.5 to 2.0  $\mu\text{L}$  of gels were placed on the patterned aluminum surface from left to right (Figure 2a). Then, four typical samples (0.5, 1.0, 1.5, and 2.0  $\mu\text{L}$ ) were selected to compare the performance with a cylindrical sample prepared using a mold. The compression tests were performed on these five samples first, as shown in Figure 2b. The strain value at 500 kPa pressure was selected to compare the pressure sensitivity of mechanical properties. All confined gels presented higher compression strain (75%, 67%, 65%, and 52% for 0.5, 1.0, 1.5, and 2.0  $\mu\text{L}$ , respectively) at 500 kPa than the cylindrical sample (strain of 38%). This indicates that less pressure can make the same deformation on the confined gels compared to the cylinder one. Then, the current change upon the applied pressure on every sample and corresponding sensitivity was measured. Similarly, all droplet-shaped samples exhibit higher sensing performance compared to the cylindrical sample (Figure 2c). At a pressure of 500 kPa, the rate of current change for the cylindrical sample is less than 300%, whereas the rate of current change for all droplet-shaped

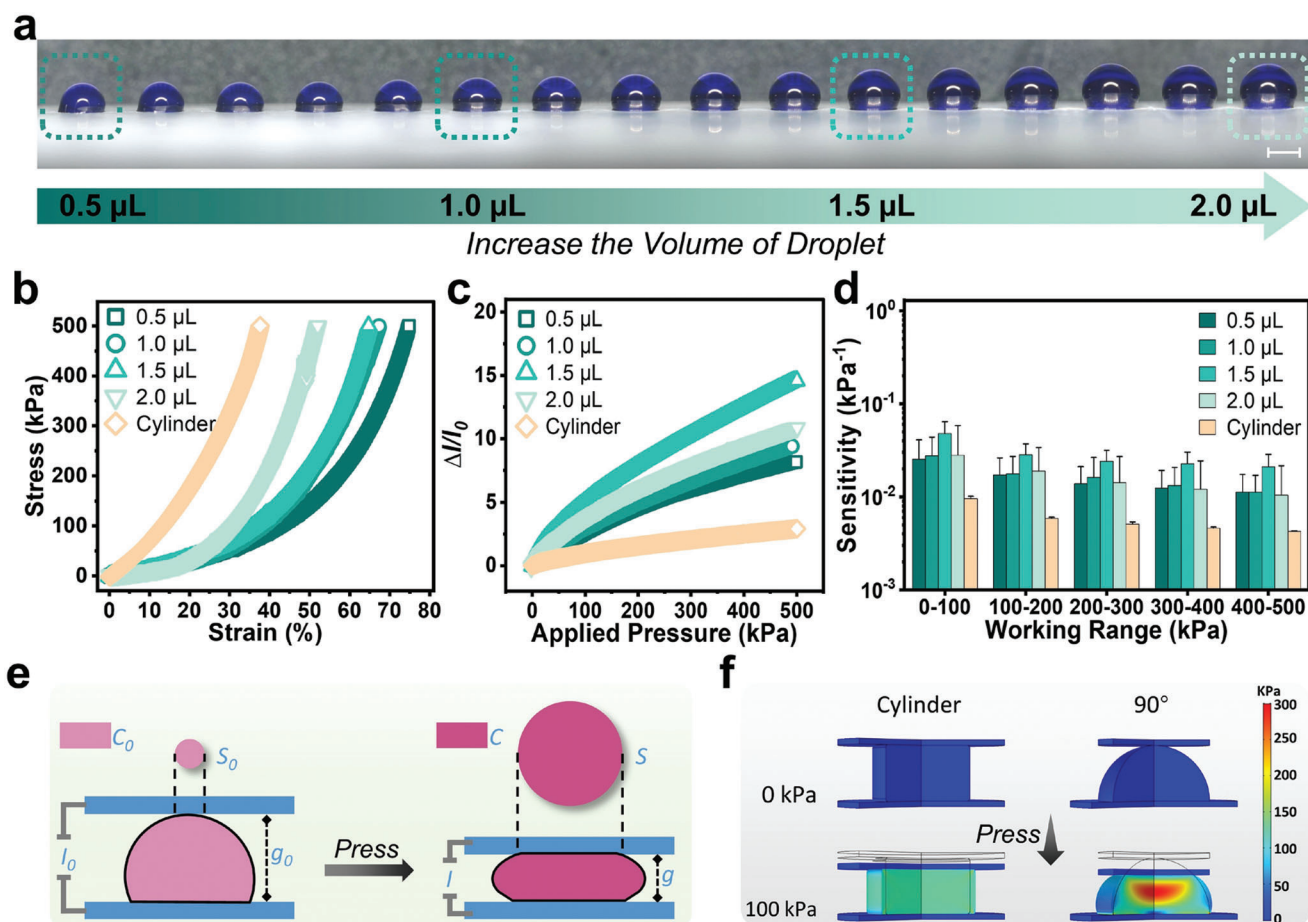


**Figure 2.** a) Photographs show conductive gel droplets on a pattern with a diameter of 1400  $\mu\text{m}$ . The volume of the droplets varies from 0.5 to 2.0  $\mu\text{L}$ . The scale bar is 1 mm. b) Representative compression stress-strain curves of conductive gels shaped from different volumes of prepolymer solution, including 0.5, 1.0, 1.5, and 2.0  $\mu\text{L}$ . The cylinder represents the bulk materials of conductive gel with a diameter of 1400  $\mu\text{m}$  and a height of 800  $\mu\text{m}$ . c) The current change ratio of fabricated pressure sensors based on conductive gels with different shapes upon applied pressure. d) The sensitivity of the obtained various pressure sensors at different working ranges. e) Schematic illustration of the sensing mechanism of the fabricated pressure sensors based on shaped conductive gels. f) Stress distribution of conductive gels with different shapes under the same engineering pressure. The shape of the wireframe is the uncompressed shape.

samples exceeds 800%. The highest current change value, generated by the 1.5  $\mu\text{L}$  sample, reaches close to 1500%, which is five times higher than the cylindrical sample. For quantitative analysis, the sensitivity of the specified current change rate, represented by the slopes of the curves corresponding to different pressure ranges, was compared (Figure 2d). Within each pressure range up to 500 kPa, the droplet-shaped samples presented higher sensitivity than a cylindrical sample, and the 1.5  $\mu\text{L}$  sample exhibited the highest average sensitivity. For pressures below 100 kPa, it reached a sensitivity of 0.048  $\text{kPa}^{-1}$ , which is 4.9 times of cylinder one. This high sensitivity is maintained after 300 compressions at 100 kPa (Figure S7, Supporting Information). We noticed an onset of degradation of the performance after about 300 compressions. Improvement of the sensor performance can be potentially realized by optimizing the formulation and network design of the polymer gel, which should enhance the mechanical stability of the gel as well as reduce evaporation kinetics.

The mechanism behind the high sensitivity of the droplet-shaped sample was further investigated. As depicted in Figure 2e,

resistive pressure sensors typically consist of conductive thin films and soft conductive materials. When compressed, the thickness of soft conductive materials decreases, resulting in a corresponding increase in current. This phenomenon can be described by the following equation.

$$I = \frac{V}{R} = \frac{V}{\frac{Cg}{S}} = \frac{VS}{Cg} \quad (1)$$

where, the abbreviations stand for voltage ( $V$ ), resistance ( $R$ ), the resistivity of the material ( $C$ ), the distance between two electrodes ( $g$ ), and the average contact area between the active materials and electrodes ( $S$ ), respectively. The sensitivity (or so-called gauge factor,  $GF$ ) of resistive pressure sensors during the low-pressure range can be expressed as follows.

$$GF = \frac{I_1 - I_0}{I_0} = \frac{1}{P} \left( \frac{S_1 g_0 C_0}{S_0 g_1 C_1} - 1 \right) \quad (2)$$

where  $P$  denotes the applied pressure. Subscripts 0 and 1 represent the value of the physical quantity without and with pressure applied, respectively. The applied pressure was set to be the same for all samples, so the sensitivity should be determined by changes in the contact area, distance, and resistivity. As shown in Movie S1, Supporting Information, the contact area between the cylindrical sample and the electrodes remains relatively constant ( $\frac{S_1}{S_0} = 1$ ), while the contact area of the droplet-shaped gel samples increases upon a decrease in the distance between electrodes ( $\frac{S_1}{S_0} > 1$ ). In terms of distance, at the same pressure, the droplet-shaped sample requires a greater strain (Figure 2b), resulting in a significantly larger  $\frac{e_0}{e_1}$  ratio compared to the cylindrical sample. The  $\frac{C_0}{C_1}$  depends on the material changes that occur during compression. The finite element analysis was conducted to study the stress distribution in the compressed samples. Since this work focuses on the droplet-shaped gel, a cylindrical sample with a similarly shaped and sized footprint contact area was taken as a reference for the primitive shape. The cylindrical sample represented the bulk gel without the structural design. Alternatively, a conical shape could be considered but their fabrication is significantly more complex in comparison with both droplet and cylindrical shapes. It was observed that the stress distribution in the cylindrical sample was uniform throughout the entire sample, while the droplet-shaped sample exhibited significant stress concentration in the middle of the half-sphere (Figure 2f). Under the same loading conditions (100 kPa), more than 25% of the droplet-shaped sample's area experienced a stress of 300 kPa, leading to a higher conductivity in that specific region. Such inhomogeneous stress distribution results in larger  $\frac{C_0}{C_1}$  in droplet-shaped samples compared to cylindrical ones. In summary, due to its unique geometry compared to the cylindrical sample, the droplet-shaped samples undergo larger changes in distance between electrodes, contact area, and resistance when subjected to applied pressure. These factors work together synergistically to contribute to its higher sensitivity.

### 2.3. Pressure Sensors Based on the Uneven Gel Array

To further enhance the pressure sensing performance, we utilized another advantage of droplet arrays. Droplets and, therefore, conductive gels of varying volumes can be conveniently assembled in a defined pattern. Building upon this advantage, an optimization approach was employed by adjusting the volumes of droplets within the array, aiming to achieve an “uneven distribution” on the whole sensing area under the applied pressure. Figure 3a and Figure S8, Supporting Information show the design philosophy of this uneven array, where four 1.5  $\mu\text{L}$  droplets form a uniform array whilst two 0.3  $\mu\text{L}$  and two 1.5  $\mu\text{L}$  droplets are staggered to form an uneven array. The comparison between the pressure sensing behavior of uniform and uneven arrays was demonstrated in Figure 3b. The remarkable enhancement in sensitivity was achieved by reducing the volume of selected droplets within a sensor array, thereby introducing unevenness into the volumes of droplet-based sensor arrays. With an applied pressure of 100 kPa, the current of the uneven array increased by 1700%, which is much higher than that of the uniform array (630%). For the sensitivity, the uneven array exhibits a two-stage, including

0–30 and 30–100 kPa (Figure 3c). The sensitivity was measured from the slope of the linear fit of the curve in a specific region. During the low-pressure region (0–30 kPa), the sensitivity of the uneven array reaches 0.29  $\text{kPa}^{-1}$ , which is three times higher than that of the uniform array (0.09  $\text{kPa}^{-1}$ ). As the applied pressure increased, the sensitivity of the uneven array maintained 0.13  $\text{kPa}^{-1}$  within 30–100 kPa, while the sensitivity of the uniform array was 0.05  $\text{kPa}^{-1}$  in the same pressure region. Such exceptional sensitivity exhibited by this uneven array method across a wide pressure range highlights its numerous advantages and advanced capabilities. To demonstrate the performance advantages of the pressure sensor in this study, a concise comparison with representative pressure sensors based on polymer gels from recent literature is presented in Figure 3d, focusing on their working pressure range and sensitivity. It is worth noting that the impressive results obtained in this study were achieved using a standard conductive gel without any specialized network design. It is expected to apply this technology to conductive materials that inherently have extremely high sensitivity. The findings underscore the versatility and efficacy of the developed array technology, showcasing its ability to surpass existing pressure sensor designs and pave the way for further advancements in the field.

### 2.4. Applications of Pressure Sensors

The excellent sensing properties of assembled gel pressure sensors make them promising for real-time monitoring of human motions. The assembled pressure sensor array was affixed to various parts of the human body using adhesive tape, enabling the detection and monitoring of a wide range of human movements and activities (Figure 4a). By placing the calibrated sensor (Figure S9, Supporting Information) on different body parts, such as the larynx, wrist, and fingers, the sensor can capture the intricate dynamics and nuances of human motion. For example, when attached to the larynx, the sensor could monitor the vibrations of the vocal cords. When the volunteer utters various letters, such as “K”, “I”, and “T”, the vocal cords produce distinct vibrations that can be captured and analyzed by the pressure sensor (Figure 4b). By examining the shape and characteristics of the current change ratio curves, it becomes possible to identify and differentiate between these spoken letters. This offers non-invasive insights into vocal cord vibrations and their relationship to speech production, enabling advancements in speech-related studies and applications.

Moreover, the high sensitivity of the array sensors at low pressures was harnessed for monitoring subtle vibrations in the human body. When attached to the wrist, the pressure sensor captured delicate fluctuations in pressure caused by periodic pulses (Figure 4c). Notably, the sensor successfully detects two distinct inflection peaks and a late systolic shoulder (as depicted in the embedded figure). This unique feature arises from the reflected waveforms originating from left ventricular contraction and the lower body. The specific values of  $P_1$  and  $P_2$  (or the enhancement index  $A = P_2/P_1$ ) serve as diagnostic indicators for assessing arterial stiffness. These compelling results underscore the potential application of the assembled gel sensor in wearable diagnostic devices, enabling real-time monitoring of vital physiological signals. In addition, the assembled pressure sensor was directly

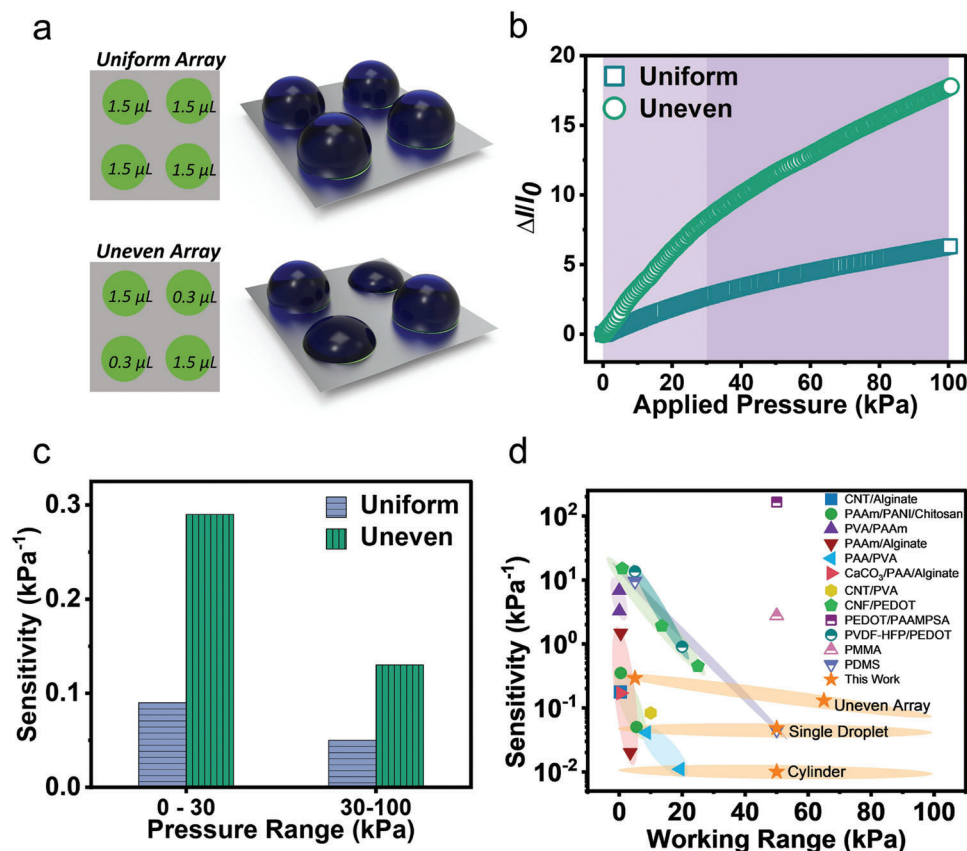


**Figure 3.** a) Schematic illustration of pressure sensor based on uniform and uneven gel arrays. The volume of every droplet is presented on the left side, which can control the shape of the gel droplet on the conductive film. b) The current change ratio of fabricated pressure sensors based on different gel arrays upon applied pressure. c) The sensitivity of the obtained pressure sensors at different working ranges. d) Comparison between this work and previously reported polymer pressure sensors in terms of sensitivity and working range. The compared polymer pressure sensors include carbon nanotube/alginate (CNT/Alginate),<sup>[37]</sup> polyacrylamide/polyaniline/chitosan (PAAm/PANI/Chitosan),<sup>[38]</sup> polyvinyl alcohol/polyacrylamide (PVA/PAAm),<sup>[39]</sup> polyacrylamide/alginate hydrogel (PAAm/Alginate),<sup>[40]</sup> polyacrylic acid/polyvinyl alcohol (PAA/PVA),<sup>[41]</sup> calcium carbonate/polyacrylic acid/alginate hydrogel (CaCO<sub>3</sub>/PAA/Alginate),<sup>[42]</sup> carbon nanotubes/polyvinyl alcohol organohydrogel (CNT/PVA),<sup>[43]</sup> cellulose nanofiber (CNF)-based aerogel with poly(3,4-ethylene dioxathiophene)/poly(styrenesulfonate) (CNF/PEDOT),<sup>[44]</sup> a conducting film consisting of (poly(3,4-ethylenedioxythiophene):poly(styrenesulfonate) and (poly(2-acrylamido-2-methyl-1-propanesulfonic acid) (PEDOT/PAAMPSA),<sup>[45]</sup> polymer nanofibers of poly(vinylidene fluoride-co-hexafluoropropene) and poly(3,4-ethylenedioxythiophene) (PVDF-HFP/PEDOT),<sup>[46]</sup> sodium hydroxide treated polymethylmethacrylate (PMMA),<sup>[47]</sup> and poly(dimethylsiloxane) (PDMS).<sup>[48]</sup>

placed on the back of the finger to monitor macro-scale human activities. By observing real-time current changes, the sensor provided insights into finger movements. Notably, when the finger was bent at angles of 15°, 30°, 60°, and 100°, the pressure sensor exhibited corresponding current changes of 18%, 42%, 75%, and 93%, respectively (Figure 4d). Such precise monitoring of macro-scale human activities has significant implications for applications in fields such as sports performance analysis, and human-computer interaction.

Finally, utilizing the advantages of the facile fabrication of this technique, we present a conductive gel array designed to detect force across a 2D plane. This breakthrough has a wide range of potential applications in the field of 2D sensing and electronic skin. By connecting a 4 × 8 array of conductive gel droplets using aluminum tape, with each droplet functioning as an independent pixel, we could further enhance the overall sensing capability of the device (Figure 4e). When an object was placed on the sensing pad, the current change profile of each gel droplet could be

captured, enabling us to create a detailed pressure distribution map (Figure 4f). This approach demonstrates the potential of the conductive gel array for precise mapping of force distribution in 2D.

### 3. Conclusion

In conclusion, this work presents a facile and efficient method for fabricating gel pressure sensors on surfaces patterned with hydrophilic regions surrounded by hydrophobic background, offering new insights into gel sensor research. The hydrophobic/hydrophilic pattern on a flexible conductive substrate successfully shapes droplets of the prepolymerization solution and maintains their confined shapes through photopolymerization. The gel sensors, composed of a crosslinked PHEMA network and a saline/ethylene glycol solvent system, exhibit mechanical and electrochemical stability. The ability to tune the shape and size of the gel droplets on the patterned surface, while maintaining



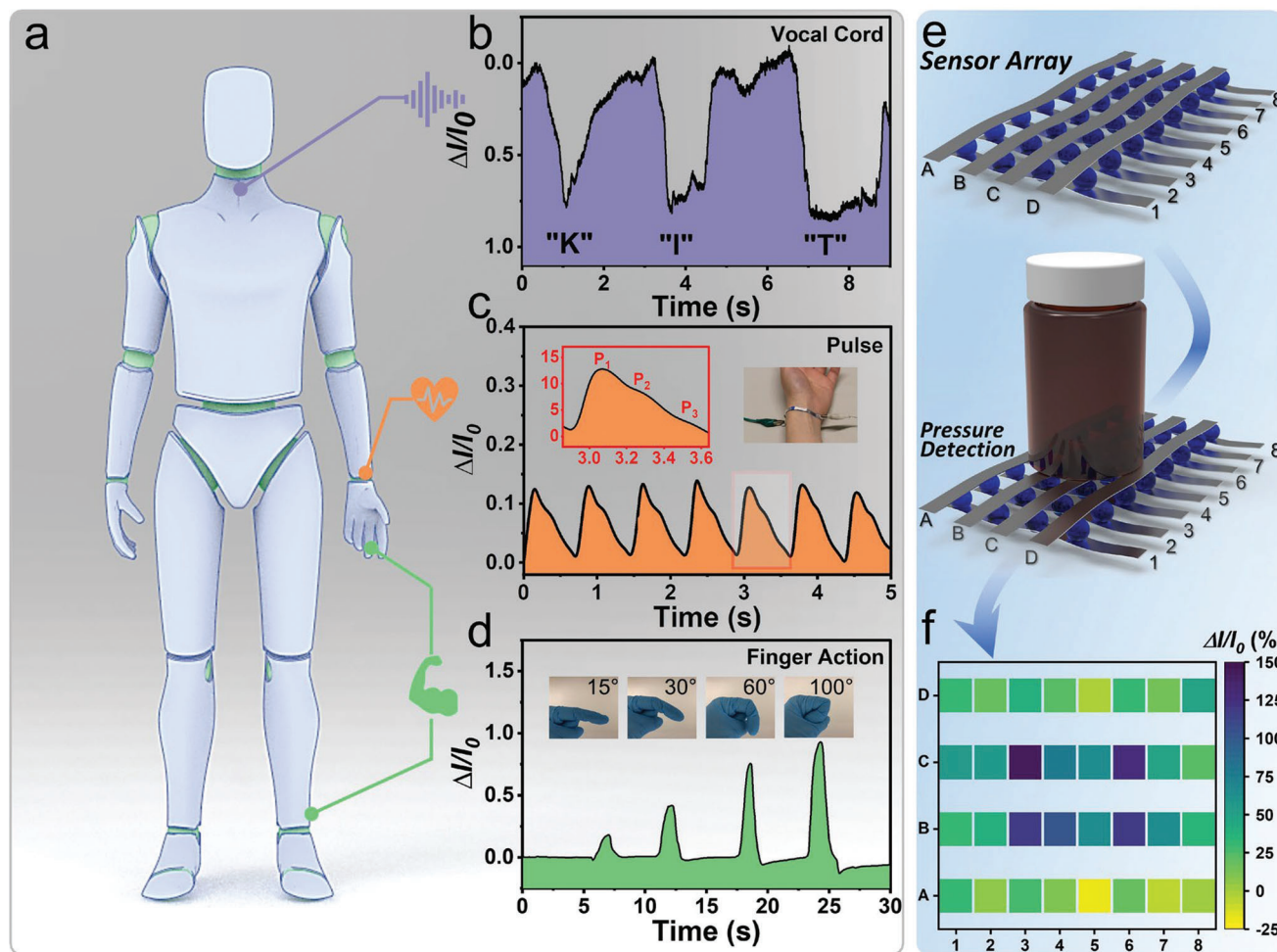


**Figure 4.** a) Schematic illustration depicts the real-time monitoring of human motions using pressure sensors based on shaped conductive gels. The specific applications shown include b) vocal cord monitoring, c) pulse detection, and d) finger movement. The shaped conductive gels enable precise sensing and measurement of these motions. e) An array of  $4 \times 8$ -shaped conductive gels is connected using aluminum tapes to form a sensing pad capable of detecting 2D area pressure. Each gel droplet functions as an individual pixel, contributing to the overall sensing capability of the pad. f) The current change of each pixel is demonstrated when a light bottle is placed on the sensing pad.

the same droplet footprint, enhances their pressure-sensing performance. Optimizing the arrangement of the gel droplets within the array results in high sensitivity within specific pressure ranges. The assembled pressure sensor demonstrates a sensitivity of  $0.29 \text{ kPa}^{-1}$  in the range of 0–30 kPa and  $0.13 \text{ kPa}^{-1}$  in the range of 30–100 kPa. These gel pressure sensors show great potential for real-time monitoring of human motions, such as vocal cord vibrations, pulse detection, or finger movements. Furthermore, leveraging the scalability of the fabrication process, a conductive gel array is successfully developed for 2D force detection. The performance of the gel pressure sensor can be further improved by optimizing the gel network structure and polymer composition in order to increase the mechanical stability, sensing resolution, and response time. The scalability, in terms of applicability to other gel systems, of this technology was confirmed by using different types of gels (Figure S10, Supporting Information). This will help for the subsequent optimization of the gel sensor. Such an efficient and straightforward method

for enhancing the sensing performance of polymer gels opens up exciting possibilities for diverse applications in wearable electronics.

## 4. Experimental Section

**Materials:** The following chemicals were used as received: ethylene glycol (EG, Sigma Aldrich), 2-hydroxyethyl methacrylate (HEMA, Sigma Aldrich), 2-hydroxy-4-(2-hydroxyethoxy)-2-methylpropiophenone (Irgacure 2959, Sigma Aldrich), poly(ethylene glycol) diacrylate (PEGDA,  $M_n \approx 250 \text{ g}\cdot\text{mol}^{-1}$ , Sigma Aldrich), sodium chloride (NaCl, Carl Roth), and trichlorovinylsilane (Sigma Aldrich). Glass slides were purchased from Schröder Spezialglas (Ellerau, Germany), and aluminum tape was obtained from 3 M.

**Patterning of Conductive Surface:** To create the conductive surface, aluminum tape was affixed to a smooth plate. The aluminum substrates were activated with an  $\text{O}_3/\text{UV}$  cleaner (Jellght Company Inc.) for 10 min, followed by treatment with trichlorovinylsilane under reduced pressure for 3 h to introduce double-bond modifications. The modified surface was then patterned by applying  $300 \mu\text{L}$  of a PFDT solution ( $400 \mu\text{L}$  of PFDT



and 40.0 mg of DMPAP in 3.600 mL of acetone) onto the surface and exposing it to UV light (366 nm, 5 mW·cm<sup>-2</sup>) for 90 s using a photomask. This triggered a thiol-ene photo-click reaction. Next, the partially fluorinated surfaces were coated with 300 μL of a solution containing 1-thioglycerol (400 μL of 1-thioglycerol and 40.0 mg of Irgacure 2959 in 1.80 mL of ethanol and 1.80 mL of water). The surfaces were then exposed to UV light (366 nm, 5 mW·cm<sup>-2</sup>) for 2 min while covered with a transparency glass, resulting in hydrophobic/hydrophilic patterned substrates. After each step, the substrates were sequentially washed with acetone and ethanol and dried using airflow.

**Patterning of Conductive Surface:** The aluminum tape was affixed to a glass slide to ensure a smooth surface during modification. After being activated with an O<sub>3</sub>/UV cleaner (Jellight Company Inc.) for 10 min, the aluminum substrates were subjected to a reaction with trichlorovinylsilane under reduced pressure for 3 h, resulting in double-bond modified substrates. The modified surface was then patterned by applying 300 μL of a PFDT solution (400 μL of PFDT and 40.0 mg of 2-dimethylamino-4-(methyl-phenylamino)-phenol in 3.600 mL of acetone) onto the surface. UV light (366 nm, 5 mW·cm<sup>-2</sup>) was then directed onto the surfaces through a designed photomask for 90 s, triggering a thiol-ene photo-click reaction. Subsequently, the partially fluorinated surfaces were covered with 300 μL of a solution containing 1-thioglycerol (400 μL of 1-thioglycerol and 40.0 mg of Irgacure 2959 in 1.80 mL of ethanol and 1.80 mL of water). The surfaces were then exposed to UV irradiation (366 nm, 5 mW·cm<sup>-2</sup>) for 2 min while covered with a transparency glass, resulting in hydrophobic/hydrophilic patterned substrates. After each step, the substrates were washed with acetone and ethanol in sequence and dried using an airflow.

**Preparation of the Conductive Gels:** To prepare the gel samples, a solution was prepared by dissolving PEGDA (50 μL) and I1173 (50 μL) in a mixture of HEMA (2.00 g), saline solution (0.9% NaCl, 1.00 g), and EG (1.00 g). The resulting prepolymer solution (200 μL) was then cured in a PTFE mold using UV irradiation (366 nm, 5 mW·cm<sup>-2</sup>) for 10 min, resulting in the formation of cylindrical samples. For the droplet-shaped samples, the prepolymer solution was carefully applied onto the hydrophilic region of a hydrophobic/hydrophilic patterned substrate and subjected to UV irradiation (366 nm, 5 mW·cm<sup>-2</sup>) for 10 min. To enhance the visual distinction of the sample shapes, methylene blue (1 mg in 2 mL of prepolymer solution) was added as a stain.

**Mechanical Characterization:** The samples were tested by using AGS-X Universal Tester (Shimadzu Inc., Japan). Three samples were prepared for each compression test. For material characterization compression tests, the samples were prepared as flat cylinders with a diameter of 10 mm and a thickness of 3 mm. For the compression tests after solvent evaporation, the dimensions of the samples were additionally measured before performing the tests. The compression speed was set at 5 mm·min<sup>-1</sup>.

**Pressure Sensing Test:** The pressure sensing properties were evaluated using the LCR-6100 (RS, UK) and AGS-X Universal Tester. The Universal Tester was responsible for applying the pressure, while the LCR meter recorded the real-time electrical resistance with a voltage of 1 V during the loading process. Prior to conducting the tests, the dimensions of the hydrogel droplets were measured. The loading speed was set at 5 mm·min<sup>-1</sup>. It was worth noting that all pressure sensing tests were conducted immediately after preparing the sensor samples unless stated otherwise. The volunteer tested by the pressure sensor was the first author of the article. These sensing tests did not require any approval from an ethics committee. The pressure corresponded to the engineering stress, which did not consider the contact area change. In the case of small devices, the pressure  $P$  was calculated by the following equation.

$$P = \frac{F}{A} \quad (3)$$

where the resisting force  $F$  is measured and the contact area  $A$  is the area of the bottom.

**Electrochemical Impedance Spectroscopy (EIS):** The EIS of the samples was conducted using Interface 1010 (Gamry, US) at a temperature of 25 °C. The frequency range employed was 105 to 0.1 Hz, with an amplitude of 10 mV. To ensure consistent conductivity measurements and pre-

vent conduction changes caused by deformation, the samples, which had a diameter of 10 mm and a thickness of 2 mm, were positioned between two stainless steel plates at a fixed distance. The ionic conductivity of the ionically conductive samples was determined using the following formula.

$$\sigma = \frac{d}{R_b A} \quad (4)$$

where,  $\sigma$  represents the ionic conductivity,  $R_b$  denotes the bulk resistance,  $d$  indicates the thickness of the flat cylindrical sample, and  $A$  corresponds to the area of the sample in contact with the measuring electrode.<sup>[49]</sup>

**Cyclic Voltammetry (CV):** The CV of samples was performed using Interface 1010 (Gamry, USA) at 25 °C in the frequency range of 10<sup>5</sup> to 0.1 Hz with an amplitude of 1 V and a scanning speed of 200 mV·s<sup>-1</sup>. To avoid electrochemical changes due to deformation, the samples (with a diameter of 10 mm and a thickness of 3 mm) were placed between two conductive plates of stainless steel at a fixed distance. No additional steps were taken to prevent evaporation of the solvent during the test.

**Photography and Contact Angle Measurements:** Microscopy images were captured using a Keyence VHX-7000 digital microscope from Japan. Digital photos were taken using a Canon EOS 80D Digital Camera. Apparent contact angles were measured using a Krüss Drop Shape Analyzer from Germany. To measure surface wetting, 2 μL droplets of deionized water were applied. Apparent contact angle measurements of gel droplets on patterned surfaces were conducted using the drop shape analyzer solely for photography and angle calculation purposes.

## Supporting Information

Supporting Information is available from the Wiley Online Library or from the author.

## Acknowledgements

Z.W. is grateful to the China Scholarship Council (CSC) for the Ph.D. scholarship. The work was further supported by the Helmholtz program BIFTM. Furthermore, the authors thank the Helmholtz Program "Materials Systems Engineering" and KIT-Center-Projekt softNeuro 2020 FE.5450.0014.5096 for their support. This project was partly supported through the Deutsche Forschungsgemeinschaft (DFG, German Research Foundation): Heisenbergprofessur (Projektnummer: 406232485, LE 2936/-91) and Germany's Excellence Strategy (2082/-1390761711, Excellence Cluster "3D Matter Made to Order").

Open access funding enabled and organized by Projekt DEAL.

## Conflict of Interest

The authors declare no conflict of interest.

## Author Contributions

Z.W. and Q.C. contributed equally to this work. Z.W. conceived and designed the experiments. Q.C. and Z.W. executed the project. Z.W., Q.C., and P.L. wrote the manuscript. All the authors discussed the results and commented on the manuscript. P.L. and Z.W. supervised this study. L.L. helped with the cyclic mechanical test and sample preparation.

## Data Availability Statement

The data that support the findings of this study are available from the corresponding author upon reasonable request.

## Keywords

droplet arrays, hydrophilic/hydrophobic patterns, patterned surfaces, polymer gels, pressure sensors

Received: June 21, 2023  
Revised: September 2, 2023  
Published online:

- [1] J. Kim, A. S. Campbell, B. E.-F. De Ávila, J. Wang, *Nat. Biotechnol.* **2019**, 37, 389.
- [2] J. Min, J. Tu, C. Xu, H. Lukas, S. Shin, Y. Yang, S. A. Solomon, D. Mukasa, W. Gao, *Chem. Rev.* **2023**, 123, 5049.
- [3] T. R. Ray, J. Choi, A. J. Bandodkar, S. Krishnan, P. Gutruf, L. Tian, R. Ghaffari, J. A. Rogers, *Chem. Rev.* **2019**, 119, 5461.
- [4] Z. Wang, H. Wei, Y. Huang, Y. Wei, J. Chen, *Chem. Soc. Rev.* **2023**, 52, 2992.
- [5] T. Strain, K. Wijndaele, P. C. Dempsey, S. J. Sharp, M. Pearce, J. Jeon, T. Lindsay, N. Wareham, S. Brage, *Nat. Med.* **2020**, 26, 1385.
- [6] M. Berggren, E. D. Głowacki, D. T. Simon, E. Stavrinidou, K. Tybrandt, *Chem. Rev.* **2022**, 122, 4826.
- [7] K. W. Cho, S.-H. Sunwoo, Y. J. Hong, J. H. Koo, J. H. Kim, S. Baik, T. Hyeon, D.-H. Kim, *Chem. Rev.* **2022**, 122, 5068.
- [8] G. Pacchioni, *Nat. Rev. Mater.* **2017**, 2, 17015.
- [9] C. Chen, J. Feng, J. Li, Y. Guo, X. Shi, H. Peng, *Chem. Rev.* **2022**, 123, 613.
- [10] C. Gu, A.-B. Jia, Y.-M. Zhang, S. X.-A. Zhang, *Chem. Rev.* **2022**, 122, 14679.
- [11] M. Lin, H. Hu, S. Zhou, S. Xu, *Nat. Rev. Mater.* **2022**, 7, 850.
- [12] R. Feiner, T. Dvir, *Nat. Rev. Mater.* **2017**, 3, 17076.
- [13] A. G. Kelly, D. O'suilleabhain, C. Gabbett, J. N. Coleman, *Nat. Rev. Mater.* **2022**, 7, 217.
- [14] C. Wang, T. Yokota, T. Someya, *Chem. Rev.* **2021**, 121, 2109.
- [15] Z. Wang, Y. Cong, J. Fu, *J. Mater. Chem. B* **2020**, 8, 3437.
- [16] J. He, Y. Zhang, R. Zhou, L. Meng, T. Chen, W. Mai, C. Pan, *J. Materials* **2020**, 6, 86.
- [17] X. Liu, J. Liu, S. Lin, X. Zhao, *Mater. Today* **2020**, 36, 102.
- [18] C. Yang, Z. Suo, *Nat. Rev. Mater.* **2018**, 3, 125.
- [19] H. Yuk, J. Wu, X. Zhao, *Nat. Rev. Mater.* **2022**, 7, 935.
- [20] P. Bertsch, M. Diba, D. J. Mooney, S. C. G. Leeuwenburgh, *Chem. Rev.* **2023**, 123, 834.
- [21] Y. Hu, *Soft Sci.* **2022**, 2, 3.
- [22] I. Apsite, S. Salehi, L. Ionov, *Chem. Rev.* **2022**, 122, 1349.
- [23] M. Cianchetti, C. Laschi, A. Menciassi, P. Dario, *Nat. Rev. Mater.* **2018**, 3, 143.
- [24] Y. Gao, Y. Wang, S. Xia, G. Gao, *Sci. China Mater.* **2021**, 64, 2313.
- [25] Y. Yu, J. Li, S. A. Solomon, J. Min, J. Tu, W. Guo, C. Xu, Y. Song, W. Gao, *Sci. Rob.* **2022**, 7, abn0495.
- [26] H. Yuk, J. Wu, X. Zhao, *Nat. Rev. Mater.* **2022**, 7, 935.
- [27] K.-H. Ha, H. Huh, Z. Li, N. Lu, *ACS Nano* **2022**, 16, 3442.
- [28] G. Ge, Y. Zhang, J. Shao, W. Wang, W. Si, W. Huang, X. Dong, *Adv. Funct. Mater.* **2018**, 28, 1802576.
- [29] K.-X. Hou, S.-P. Zhao, D.-P. Wang, P.-C. Zhao, C.-H. Li, J.-L. Zuo, *Adv. Funct. Mater.* **2021**, 31, 31.
- [30] H. Peng, Y. Xin, J. Xu, H. Liu, J. Zhang, *Mater. Horiz.* **2019**, 6, 618.
- [31] X. Pei, H. Zhang, Y. Zhou, L. Zhou, J. Fu, *Mater. Horiz.* **2020**, 7, 1872.
- [32] B. C.-K. Tee, A. Chortos, R. R. Dunn, G. Schwartz, E. Eason, Z. Bao, *Adv. Funct. Mater.* **2014**, 24, 5427.
- [33] S. R. A. Ruth, V. R. Feig, H. Tran, Z. Bao, *Adv. Funct. Mater.* **2020**, 30, 30.
- [34] Z. Huang, G. Shao, L. Li, *Prog. Mater. Sci.* **2023**, 131, 101020.
- [35] M. Su, Y. Song, *Chem. Rev.* **2022**, 122, 5144.
- [36] H. Yin, Y. Zhu, K. Youssef, Z. Yu, Q. Pei, *Adv. Mater.* **2022**, 34, 2106184.
- [37] Y. Tai, M. Mülle, I. Aguilar Ventura, G. Lubineau, *Nanoscale* **2015**, 7, 14766.
- [38] J. Duan, X. Liang, J. Guo, K. Zhu, L. Zhang, *Adv. Mater.* **2016**, 28, 8037.
- [39] G. Ge, Y. Zhang, J. Shao, W. Wang, W. Si, W. Huang, X. Dong, *Adv. Funct. Mater.* **2018**, 28, 1802576.
- [40] X. Zhang, N. Sheng, L. Wang, Y. Tan, C. Liu, Y. Xia, Z. Nie, K. Sui, *Mater. Horiz.* **2019**, 6, 326.
- [41] G. Ge, W. Yuan, W. Zhao, Y. Lu, Y. Zhang, W. Wang, P. Chen, W. Huang, W. Si, X. Dong, *J. Mater. Chem. A* **2019**, 7, 5949.
- [42] Z. Lei, Q. Wang, S. Sun, W. Zhu, P. Wu, *Adv. Mater.* **2017**, 29, 1700321.
- [43] W. Zheng, L. Xu, Y. Li, Y. Huang, B. Li, Z. Jiang, G. Gao, *J. Colloid Interface Sci.* **2021**, 594, 584.
- [44] Y. Wu, Z. Yan, T. Wang, J. Wang, T. Wang, Z. Hu, Y. Ao, Y. Wang, M. Li, *ACS Appl. Polym. Mater.* **2023**, 5, 3938.
- [45] X. Su, X. Wu, S. Chen, A. M. Nedumaran, M. Stephen, K. Hou, B. Czarny, W. L. Leong, *Adv. Mater.* **2022**, 34, 2200682.
- [46] O. Y. Kweon, S. J. Lee, J. H. Oh, *NPG Asia Mater.* **2018**, 10, 540.
- [47] S. Chen, S. Peng, W. Sun, G. Gu, Q. Zhang, X. Guo, *Adv. Mater. Technol.* **2019**, 4, 1800681.
- [48] L. Singh, K. Tripathy, M. Bhattacharjee, *Adv. Eng. Mater.* **2022**, 24, 2200500.
- [49] X. Qian, N. Gu, Z. Cheng, X. Yang, E. Wang, S. Dong, *J. Solid State Electrochem.* **2001**, 6, 8.